Recent Changes in the Microwave Scattering Properties of the Antarctic Ice Sheet

Andrew W. Bingham and Mark R. Drinkwater, *Member, IEEE*

***Abstract*—Time series, satellite microwave data are used to monitor and quantify changes in the scattering properties of the Antarctic ice sheet. Daily ERS scatterometer (EScat) and Special Sensor Microwave/Imager (SSM/I) image data, acquired since 1992, are analyzed to understand the seasonal and interannual changes over the ice sheet. For regions of the ice sheet where azimuthal modulation is negligible, seasonal cycles are observed in both the EScat (amplitude $\sim$0.5 dB) and SSM/I data (amplitude $\sim$ 10 K). These cycles are attributed to seasonal changes in surface temperature. Interannual variability in the time series signatures appears to be associated with accumulation. There is also evidence to suggest that shifts in the wind direction can alter the backscatter through azimuthal modulation. Over the period 1992–97, large trends are observed in the EScat (< -0.3 dB yr^{-1}) and SSM/I (>1 K yr^{-1}) signatures over several regions in Antarctica. These changes typically occur over ice shelves and at the margins of the ice sheet where previous melt events have occurred, and where accumulation is relatively high (>300 mm yr^{-1}). It is likely the large changes result from the successive burial of an efficient scattering layer formed by refreezing after a melt event prior to 1992. There is also evidence to suggest that similarly large changes can be observed in the interior of the ice sheet due to the burial of depth hoar layers. In order to monitor long term change in the properties of the Antarctic ice sheet, it is necessary to remove the seasonal cycle from time series microwave data. Such anomaly data can then be used to understand the link between EScat and SSM/I with accumulation and wind shifts.**

***Index Terms*—Antarctica, azimuthal anisotropy, backscatter, climate change, emission, ice sheet, interannual change, radar, radiometer, scatterometer, seasonal change.**

I. Introduction

THE ANTARCTIC ice sheet plays an important role in the climate system, yet little is known about how it changes in response to local and global climate forcing. A variety of studies have demonstrated that Antarctica is experiencing change. Direct observations of ice shelves on the Antarctic Peninsula during the past fifty years show an overall retreat [1], [2]. The extent and duration of the summer melt season on the peninsula have been estimated from satellite passive microwave data, indicating summer melting increased by about one day per year between 1978 and 1991 [3]. On the West Antarctic ice sheet, dramatic changes have been observed by comparing satellite visible imagery acquired in 1963 with recently acquired imagery [4] and by radar interferometry [5]. On a broader scale, recent comparisons of Ku-band scatterometer images of Antarctica acquired in 1978 and 1996 from the Seasat and NASA Scatterometer (NScat) satellite missions, respectively, demonstrated that significant changes have occurred during the intervening 18 years [6]. Whether such changes are a result of possible global warming, as predicted by Mercer [7], or due to changes in large-scale meteorological forcing resulting from some other naturally occurring phenomenon such as the eight-year Antarctic circumpolar wave [8] needs to be established. This can only be achieved effectively by frequent, long-term, Antarctic-wide observations.

Microwave satellite remote sensing is a practical way of monitoring long-term changes in the properties of the entire Antarctic ice sheet. Data acquired from microwave instruments can be acquired day and night in all weather conditions and provides detailed information on the surface and subsurface of polar glaciers and ice sheets [9], [10]. Synthetic aperture radar (SAR) image data have a high resolution, but the spatiotemporal coverage that can be accomplished is extremely limited. Scatterometer image data have a greater spatial and more frequent coverage, albeit at a lower spatial resolution, making this instrument ideal for monitoring the Antarctic ice sheet. Moreover, these data complement passive microwave radiometer (PMR) image data. Together, they provide a valuable data set for studying change in Antarctica.

The aim of this study is to quantify changes in the surface properties of the Antarctic ice sheet using C-band (5.3 GHz) EScat, Ku-band (13.6 GHz) NScat and Seasat and multichannel (19–85 GHz) Special Sensor Microwave/Imager (SSM/I) PMR time series image data. We quantify and attempt to explain the observed seasonal and interannual variability in microwave signatures over a region where negligible long-term change has occurred (e.g., Ronne Ice Shelf). We also examine regions with differing glaciological and meteorological characteristics. Finally, the extent of change in scattering properties on the entire Antarctic ice sheet since 1992 is quantified, and we relate these changes to changes in the geophysical properties of the ice sheet.

II. Microwave Imaging of Ice Sheets

Microwave image data of Antarctica have been routinely collected by ERS-1 and 2 scatterometers (EScat) since 1991 and by SSM/I PMR instruments since 1978. A short record of Ku-band Seasat scatterometer (SASS) and NScat image data are also available. SASS operated for 100 days, between June and October, 1978, and NScat operated for 10 months between August, 1996 and June, 1997, before the ADEOS platform failed.

Manuscript received April 27, 1999; revised January 3, 2000. This work was suppported in part by a National Research Council/Resident Research Associateship Award and in part by Code YS, National Aeronautics and Space Administration (NASA), Washington, DC.

The authors are with the Jet Propulsion Laboratory, California Institute of Technology, Pasadena, CA 91109 USA (e-mail: awb@pacific.jpl.nasa.gov).

Publisher Item Identifier S 0196-2892(00)05527-3.

The EScat instrument (launched on ERS-1 in July 1991 and ERS-2 in April 1995) measures VV-polarized normalized radar cross-section backscatter σ^0 at various azimuth and incidence angles along a 500 km-wide swath. A continuous dataset of Antarctica has been successfully compiled from 1991 to the present day, comprising gridded data with 25-km pixel spacing and an estimated intrinsic resolution of 50 km. The only measurement conflict is that the scatterometer subsystem of the Active Microwave Instrument (AMI) is periodically switched off during competing SAR-mode operation. This results in some scatterometer data gaps in the vicinity of operable Antarctic SAR receiving stations (most significantly, over the tip of the Antarctic Peninsula and at locations within 200 km of McMurdo Station).

In this study, we have utilized enhanced resolution EScat image data processed with the scatterometer image reconstruction with a filtering (SIRF) algorithm [11]. Briefly, over glacial ice, σ^0 (in dB) is approximated as a linear function of the incidence angle θ in the range $20^\circ \leq \theta \leq 55^\circ$ [12]

$$\sigma^\circ(\theta) = A + B(\theta - 40) \tag{1}$$

where the coefficients A and B depend on surface characteristics, polarization, and azimuth angle. A is the expected value of σ^0 at 40° (mid-swath) incidence, and B describes the variation of σ^0 with θ. The SIRF algorithm uses multiple, overlapping measurements of σ^0 and postprocessing to create enhanced resolution, temporally averaged image data of A and B [11]. As a tradeoff between resolution and temporal averaging, six-day averaged images are derived at three-day intervals, with an estimated resolution of ~25 km, resampled onto a polar-stereographic grid with 8.8-km pixel spacing.

The SSM/I is a four-frequency (85.5, 37.0, 22.2, and 19.3 GHz) linearly dual-polarized passive microwave radiometric system mounted on the Defense Meteorological Satellite Program (DMSP) F8 (launched on July 1987), F10 (November, 1990), F11 (December, 1991), F12 (August, 1994) and F13 (March, 1995) platforms. Daily polar-stereographic gridded brightness temperature (T_b) image data are processed and distributed by the National Snow and Ice Data Center (NSIDC), Boulder, CO. Swath data for each 24 h period are mapped to respective grid cells using a "drop in the bucket" sum and average method. 85.5-GHz data are gridded at a pixel spacing of 12.5 × 12.5 km and all other channels at a pixel spacing of 25 × 25 km.

Much is already known about the mechanisms that control microwave signatures of snow and ice surfaces. In general, microwave signatures are dependent on absorption and scattering losses within the firn pack [13]. For dry, fine-grained firn, absorption and scattering losses are typically small. As a consequence, the penetration depth is on the order of a few hundred times the wavelength (Fig. 1). For coarse-grained firn, however, or at high frequencies (> 94 GHz), scattering losses become significant. In this case, the penetration depth is significantly reduced, as quantified in Fig. 1. In terms of microwave signatures, regions consisting of coarse-grained firn have a higher backscatter coefficient and lower brightness temperature than regions of fine-grained firn. Enhanced volume scattering directly influences the backscatter, while brightness temperature decreases because emissivity decreases in accordance with the Rayleigh-Jeans approximation at microwave frequencies $T_b(\lambda) = \epsilon T_p$, where ϵ is the microwave emissivity, and T_p is the effective physical temperature of the snow [10].

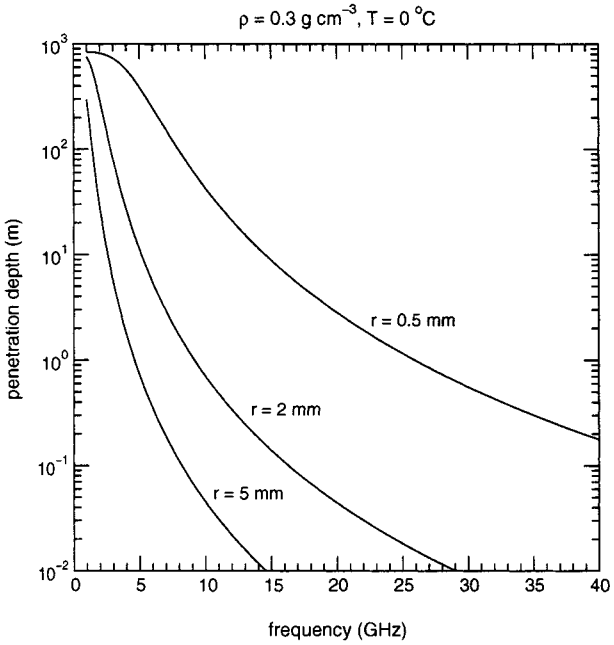

Fig. 1. Theoretical microwave penetration depth for snow with a density of 0.3 g cm^{-3} at a temperature 0° C with different grain radii. In computing the frequency response, we assumed a Rayleigh scattering model (e.g., [22]).

For wet snow, the presence of liquid water results in high absorption losses that reduce the penetration depth to the order of one wavelength [15]. Volume scattering becomes negligible, resulting in a strong reduction in backscatter and an increase in the brightness temperature due to near-blackbody emission. When wet snow refreezes, the mean grain size increases, partly because smaller grains tend to melt before larger ones, and partly because grains bond together through enhanced packing [16]. In addition, water that percolates through the snow and refreezes can form ice lenses and ice glands. The result is a significant enhancement in volume scattering after refreezing and consequently, an increase in backscatter and decrease in brightness temperature [10].

In Antarctica, the firn pack is characterized by annual and seasonal layering [17]–[19], which adds a further complexity to the interpretation of microwave signatures. Results from multilayered scattering models [20], [21] demonstrate that hoar layers and refrozen melt layers have a major impact on microwave signatures. Indeed, the presence of a strong scattering layer close to the surface reduces the penetration depth to the upper few centimeters of the firn pack. This is particularly true at the SSM/I frequencies.

Changes in microwave signatures under different meteorological and glaciological conditions have been used to study different aspects of the polar ice sheets. PMR observations have been used to investigate the spatial and temporal extent of hoar and melt on the Greenland ice sheet [23]–[25] and the Antarctic ice sheet [3], [26]. High resolution SAR imagery has

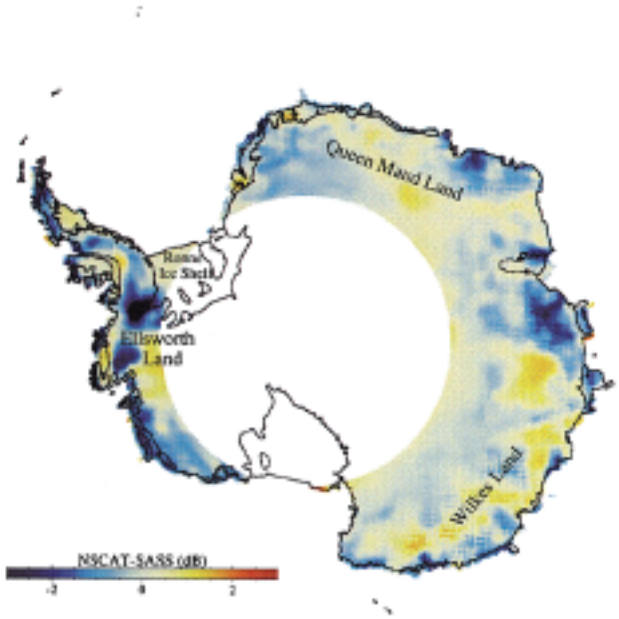

Fig. 2. NScat-SASS A difference image for the same September 23–28 six-day period in 1996 and 1978, respectively. The large data hole centered at the south pole occurs because SASS had a coverage to only 72° S. Furthermore, the high spatial-frequency variability is attributed to relatively poor SASS sampling. Image courtesy of Drinkwater and Long [6].

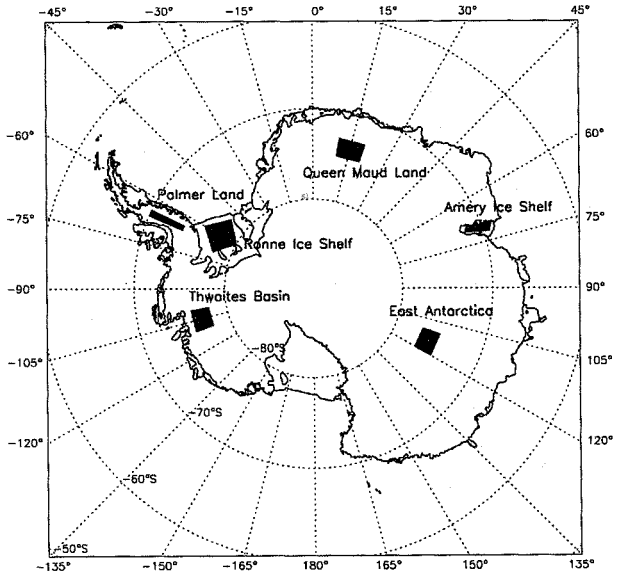

Fig. 3. Locations of regions of study on Antarctica.

been used to map surface facies on the Greenland ice sheet [27] and other Arctic ice caps (e.g., [28]). The potential of SIRF-processed scatterometer data sets for ice sheet-related research has also been demonstrated [12], [29]. Drinkwater and Long [6] documented decadal changes in Ku-band backscatter on the Antarctic ice sheet by differencing NScat and SASS SIRF image data for the same winter period. It is possible to make this comparison because the two instruments are identical in frequency and polarization, and differences between the viewing geometry are only minor. The results of this study are presented Fig. 2 which shows the 18-year difference between A images acquired during late September of the SASS and NScat missions. There are a number of regions on the ice sheet where dramatic changes occurred. In Ellsworth Land (Fig. 2) reductions of 3 dB or more are observed, particularly in the location of the Evans Ice Stream (75° 20′S 77° W) and Pine Island Glacier basin (75° S 102° W) (Fig. 3). In contrast, large-scale increases of up to 2 dB are observed at higher elevations in Wilkes Land (Fig. 2) between elevations of approximately 1 and 3 km, Queen Maud Land (Fig. 2) and at lower latitudes in Ellsworth Land. Drinkwater and Long [6] have speculated that these regionally confined areas of large changes are attributable to combinations of changes in patterns of snow accumulation and long-term variations in katabatic wind regimes. The effects of the latter are particularly important because alignment of meter-scale surface features can account for azimuthal modulations of several dB's in these Ku-band scatterometer data [30]. In regions of strong katabatic winds, seasonal realignment in surface elements such as sastrugi may therefore be responsible for some differences between NScat and SASS. This is particularly true in Wilkes Land, where Long and Drinkwater [30] note strong azimuthal modulation as a result of well-developed sastrugi resulting from the intense katabatic wind regime. In this paper, however, to avoid influences of anisotropic backscatter, study regions were selected where azimuthal modulation is negligible based on the results in [30].

III. Seasonal Changes

A. Data Analysis

Time-series EScat and SSM/I data from a number of glaciologically distinct regions in Antarctica (ice shelves, ice streams, and regions of low and high accumulation) have been analyzed for the period 1992–1997. Pixel averaged EScat-A and SSM/I 19V T_b signatures for six different regions (Fig. 3) are presented in Fig. 4. The data presented in this figure have not been normalized in order to emphasize the time-varying signature for each of the areas of interest. The EScat record is incomplete at the beginning of 1992 because the AMI-operated predominately in SAR-mode and therefore, insufficient data were collected for the SIRF algorithm to produce reliable image data. Between July 1997 and the present, SIRF image data are temporarily unavailable.

For all regions, A and T_b signatures contain a seasonal cycle and in some cases, there is evidence of an interannual signal. Typically, the seasonal cycle in the A and T_b signatures has an amplitude of ∼0.5 dB and ∼10 K, respectively. An interannual trend can be observed in the A signatures of Palmer Land, Amery Ice Shelf, and Thwaites Basin, while a trend in T_b is seen only in the Amery Ice Shelf data (Fig. 4).

A number of data "spikes" are observed in the A signatures that are probably related to short-term changes in the firn pack characteristics. Negative spikes in A occur over test sites near the coast and during the austral summer season, which suggests melting is the principal mechanism. Over the Amery Ice Shelf, the T_b data also show a marked peak during the summer.

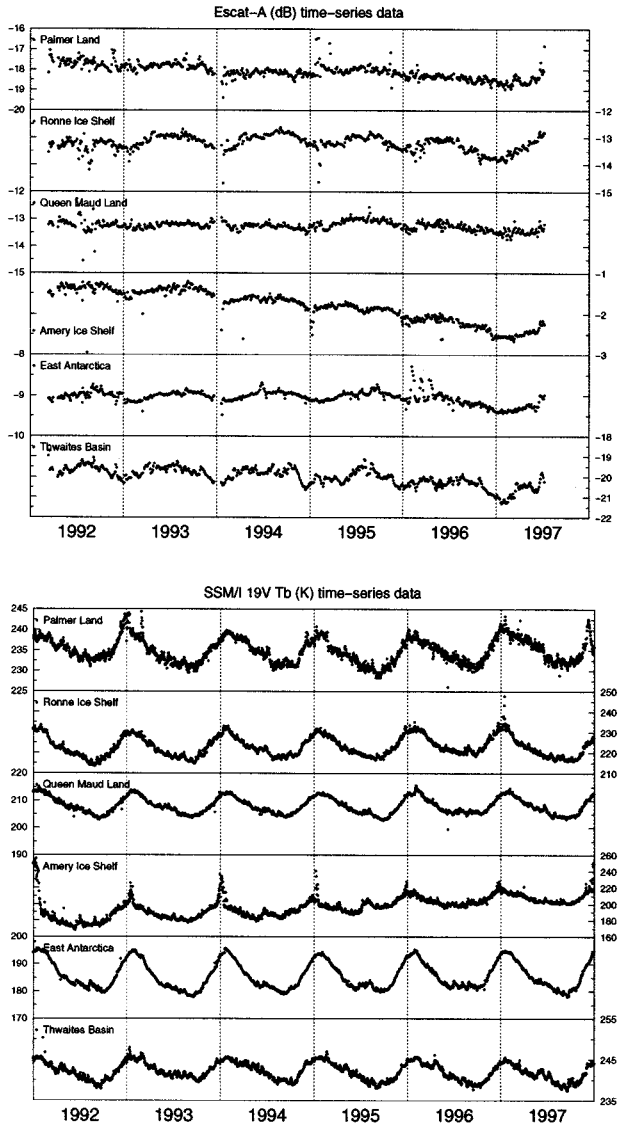

Fig. 4. Time-series of EScat A (in dB) (top) and SSM/I 19V T_b (in K) (bottom) for the six regions of interest shown in Fig. 3. Note, we have used different scales between the six regions in order to emphasize the seasonal time-varying signals.

This peak is likely caused by near-black body emission in some pixels within the sample region, indicating the presence of liquid water. While the T_b data show melting occurs for as much as 20 days, the A data captures only a few samples of melting because of the tradeoff between spatial and temporal resolution in the SIRF algorithm. Nevertheless, the A data captures possible melt events on Palmer Land and the Ronne Ice Shelf, which are not apparent in the T_b data. In this case, it is possible that melting is confined to a small region and therefore does not impact the low spatial resolution SSM/I data.

Positive spikes in A are observed over Palmer Land during the Autumn 1995 and over East Antarctica during Autumn 1996. Over Palmer Land, there is a corresponding drop in T_b of about 5K. This is probably linked to the formation of hoar crystals, which are susceptible to formation during autumn when high temperature gradients exist within the firn pack. As discussed in the previous section, hoar crystals enhance microwave scattering, resulting in an increase in A and a decrease in T_b. Over

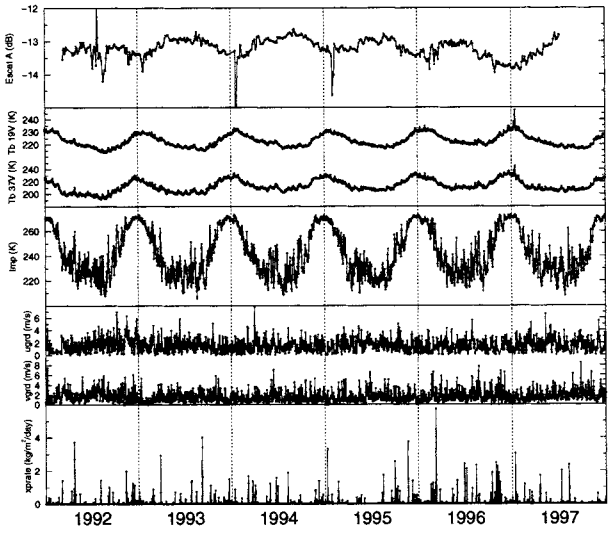

Fig. 5. Ronne Ice Shelf time-series data of (a) EScat A values, (b) SSM/I 19V T_b, (c) SSM/I 37V T_b, (d) NCEP surface temperature (T_s), (e) NCEP zonal wind speed $(ugrd)$, NCEP meridional wind speed $(vgrd)$), and (d) NCEP precipitation rate PRATE.

East Antarctica there is no corresponding change in T_b. Again, this may be an issue related to the low spatial resolution of SSM/I, or alternatively, this may be linked to changes in surface roughness at the C-band scale.

Despite increases in air temperatures on the Antarctic Peninsula over the past 50 years [31], evidence from Fig. 2 suggests that the Ronne Ice Shelf experienced no significant long-term change and is therefore an appropriate region to study seasonal variability in microwave signatures. Mean A and T_b time-series signatures for a 1° box positioned over the interior of the Ronne Ice Shelf (Fig. 3) are presented in Fig. 5, along with surface temperature (T_s), zonal wind $(ugrd)$, meridional wind $(vgrd)$, and precipitation rate PRATE, which have been obtained from the National Center for Environmental Prediction/National Center for Atmospheric Research (NCEP/NCAR), Boulder, CO, reanalysis time-series atmospheric data set.

We note a strong correlation between the satellite measurements and surface temperature. The correlation coefficient is -0.58 between A and T_s, and 0.84 between T_b and T_s. The satellite measurements show no correlation with $ugrd$, $vgrd$, and PRATE. This suggests that the observed microwave seasonal cycle is predominately driven by seasonal variations in surface temperature. This result is also consistent with comparisons made between Automatic Weather Station (AWS) air temperature and SSM/I T_b data of the Greenland ice sheet [32]. As a check to ensure azimuthal modulation is not contributing to the seasonal cycle, we used the procedure outlined in Long and Drinkwater [30] for data acquired during the 1996 austral winter. The results show a maximum azimuthal modulation of $\pm$ 0.16 dB (at $\theta = 40°$) for typical seasonal shifts in the wind direction of $\pm$ 5°). Furthermore, our preliminary studies suggest that over regions where azimuthal modulation is most pronounced (i.e., Wilkes Land) the temporal variation is linked to synoptic time-scale processes as opposed to seasonal time-scale processes.

B. Modeling Seasonal Change

In order to demonstrate how temperature impacts microwave signatures, we have utilized simple radiative transfer models that incorporated readily observable parameters for predicting A and T_b from layered Antarctic firn. We recognize that in absolute terms, the models we have used are not the most sophisticated. Nevertheless, these models permit us to generalize the scattering problem and support our hypotheses.

The total backscatter from dry Antarctic firn is considered as the incoherent sum of the isotropic volume backscattering components from each layer within the firn pack. Rough-surface scattering effects are neglected at air-firn and firn-firn boundaries, as the impedance mismatch between firn layers reflection coefficient is small [33]. Following the methodology developed in Bingham and Drinkwater [21], the total backscatter σ_T^0 at an incidence angle θ_0 is given by

$$\sigma_T^0 = \Upsilon_{0,1}^2 \sigma_{v1}^0(\theta_0) + \sum_{j=2}^{n} \frac{\prod_{i=1}^{j-1} \Upsilon_{i,i+1}^2(\theta_i)}{\prod_{i=1}^{j-1} L_i^2(\theta_i)} \sigma_{vj}(\theta_j) \quad (2)$$

where

- σ_{vj}^0 volume scattering coefficient from the jth layer;
- θ_j refracted incidence angle in the jth layer, computed using Snell's law;
- $\Upsilon_{j,j+1}$ power transmission coefficient at the jth and $j+1$th layer;
- L_j one-way power loss factor across the jth layer.

The volume scattering coefficient is modeled as the sum of independent spherical Rayleigh scatterers (ice grains in firn) [22], [34]. Using this approach, volume scattering is treated as a function of grain radius, firn density, and dielectric constant which, in turn, is related to density and temperature [35].

In order to compute brightness temperature of a multilayered Antarctic firn surface, we have adapted the model of [36]. Emission from each layer is assumed proportional to the mean layer temperature T_j, and this is summed over N layers such that the brightness temperature is given by

$$T_b(\theta_0) = \sum_{j=1}^{N} T_j (1 - 1/L_j(\theta_i))(1 + \Gamma_{j+1}/L_j(\theta_i)) \cdot \prod_{i=1}^{j} (1 - \Gamma_i(\theta_i)) \cdot \prod_{i=2}^{j} L_{j-1}(\theta_i) + T_{atm} \quad (3)$$

where $\Gamma(\theta)$ is the power reflection coefficient, and T_{atm} accounts for atmospheric effects.

Input to both models are depth profiles of firn density, grain radius, and temperature. Over the area of the satellite footprint, each of these profiles can vary considerably. We therefore use standard relationships between each of the parameters and depth and assume these relationships represent the "average" profile over the satellite footprint.

Firn density ρ is assumed to increase exponentially with depth. Analysis of ice cores from Dome C, Antarctica, by Alley *et al.* [37] indicate that the density variation with depth (in g cm^{-3}) for an average density profile is

$$\rho(z) = 0.922 - 0.564 \exp(-0.0165z). \quad (4)$$

For fine-grain firn the density variation with depth is

$$\rho(z) = 0.922 - 0.491 \exp(-0.0133z) \quad (5)$$

and for coarse-grain firn is is

$$\rho(z) = 0.922 - 0.573 \exp(-0.0163z). \quad (6)$$

Grain-radius profile is determined by assuming the cross-sectional area of a grain increases linearly with time, such that $C = C_0 + Kt$, where C_0 is the cross-sectional area at time zero, K is the crystal growth rate (typical value is 0.000 42 mm^2 yr^{-1} [37]), and t is time. Assuming a mean annual layer of thickness D, the depth-dependent grain radius $r(z)$ is given by

$$r(z)^2 = r_0^2 + Kz/(\pi D) \quad (7)$$

where r_0 is the mean radius at the surface. Other studies have also shown that a cubic relationship is valid (e.g., [14]). Firn-layer temperature is computed using conventional heat-conduction theory. Assuming a sinusoidal seasonal surface temperature of the form $T_s = T_m + T_a \sin(w(t - \phi))$, where T_m and T_a is mean temperature and seasonal amplitude, respectively, w is frequency, t is time, and ϕ is phase, the temperature profile with depth is given by

$$T(z,t) = T_m + T_a \exp\left(-z(w/2k)^{1/2}\right) \cdot \sin\left(w(t - \phi) - z(w/2k)^{1/2}\right). \quad (8)$$

k is the thermal diffusivity of snow, which is related to the thermal conductivity κ, density and specific heat capacity γ, (2009 J kg^{-1}K^{-1}) by $k = \kappa/\rho(z)\gamma$. Using data from 27 studies on the thermal conductivity of snow, Sturm *et al.* [38] have derived a quadratic relationship

$$\kappa = 0.138 - 1.01\rho + 3.233\rho^2 \quad \text{if } 0.156 \le \rho \le 0.6,$$
$$\kappa = 0.023 + 0.234\rho \quad \text{if } \rho < 0.156 \quad (9)$$

where ρ is in g/cm^3 and κ is in Wm^{-1}K^{-1}.

Modeled A and T_b signatures for the Ronne Ice Shelf are compared with satellite-observed values in Fig. 6. In computing the signatures, we set the layer thickness to a fixed value of $D = 50$ mm [39] and assumed an average density depth profile (4). Surface temperature forcing was based on the best fit to the seasonally-varying NCEP surface temperature data presented in Fig. 5

$$T(0,t) = -24.7 + 19.2 \sin\left(\frac{2\pi}{366.3}(t + 93.4)\right). \quad (10)$$

In addition, the error or offset between modeled and observed signatures was minimized by adjusting the parameters r_0 and T_{atm}. The best fit was achieved with a surface grain radius of $r_0 = 0.26$ mm and $T_{atm} = -7.1^\circ$ C. These values appear to be consistent with *in situ* data. For example, Higham and Craven [39] have found that the average grain radius in the upper 2

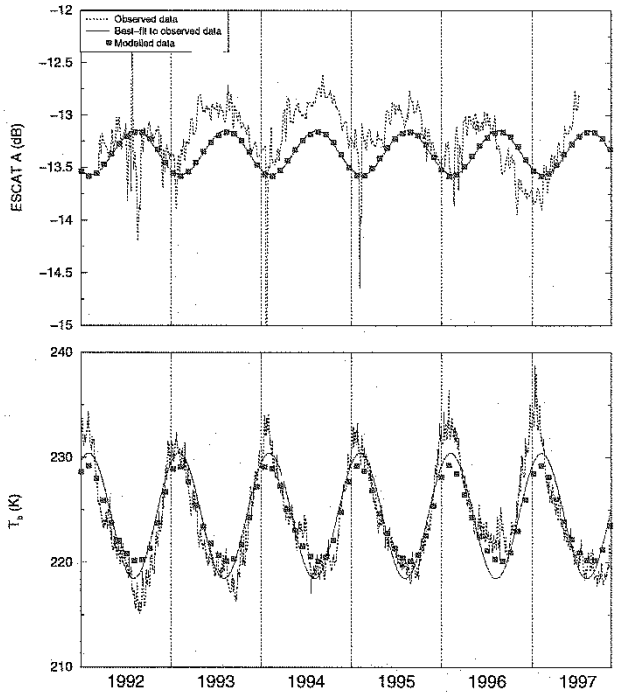

Fig. 6. Comparison between observed and modeled signatures for the Ronne Ice Shelf, using seasonally modulated surface temperature forcing (10), with fixed firn layer thickness ($D = 50$ mm) and depth-dependent density (4), grain radius (7), and temperature (8) profiles. A best fit between the observed and model values was obtained with $r_0 = 0.26$ mm and $T_{atm} = -7.1^{\circ}$ C.

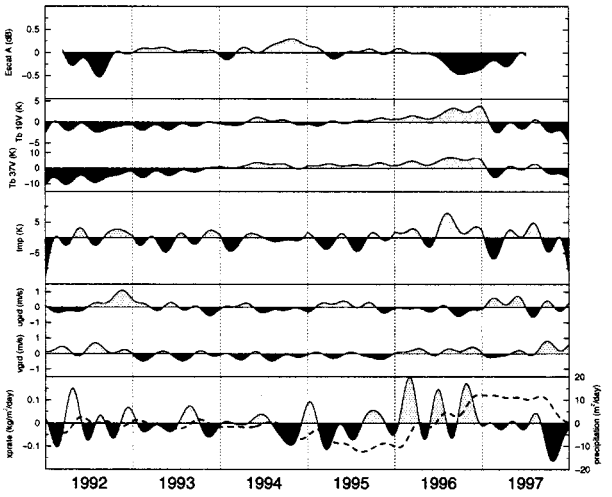

Fig. 7. Time-series anomaly data (i.e., mean annual cycle removed) for the Ronne Ice Shelf. Positive anomalies (shaded light) are above average, and negative anomalies (shaded dark) are below average. Note, short-term weather effects have been removed by smoothing the input time-series data (Fig. 5) with a 100-day low-pass filter prior to computing the anomalies. Furthermore, the mean annual cycle was computed between 1992 and 1997 for all data sets, with exception to EScat-A, which was computed between 1993 and 1996. Anomalies in the total precipitation have been computed by integrating the PRATE anomaly time-series data.

m of Antarctic firn is less than 0.75 mm. Resulting modeled signatures are almost identical to the mean annual microwave signature cycle (computed as a best-fit to seasonal means of A and T_b values). This result supports our contention that thermal forcing is the primary external factor driving seasonal variability in A and T_b , by altering the scattering, absorption, and emission properties of the firn layers.

C. Seasonal Anomalies

The mean seasonal cycle in A and T_b can be explained by variations in the mean seasonal air and firn temperatures. However, in Fig. 6, there are clear anomalies between the observed time-series microwave signatures and the corresponding mean seasonal cycle. These anomalies, along with the NCEP/NCAR anomaly data for the Ronne Ice Shelf, are presented in Fig. 7. Time-series anomalies are constructed by removing a mean annual cycle from the time-series data (Fig. 5). In this case, the data is smoothed to suppress weather effects using a 100-day, low-pass filter, and a mean annual cycle computed for the period 1992 and 1997 for all data fields except EScat, which was averaged between 1993 and 1996.

A multiple cross-correlation analysis between the satellite and NCEP/NCAR anomaly data (Fig. 7) reveals that A anomalies are mostly correlated to precipitation (P) anomalies ($r = -0.52$), while T_b anomalies are correlated to temperature anomalies ($r = 0.58$). This is especially noticeable in 1996 when T_s and P anomalies were consistently positive, probably as a result enhanced cyclonic activity in the Weddell Sea bringing warm and moist air onto the ice shelf. Variations in snow accumulation are expected to have a significant impact on layer thickness, mean grain size, and snow density. It is likely, therefore, that an increase in accumulation, as observed in the 1996 data, lays down snow layers that are thicker than normal and hence, cause a reduction in A by enhanced absorption of microwave energy. In this case, an increase in T_b due to enhanced emission would also be expected [14], but our analysis shows little correlation between T_b and precipitation ($r = 0.12$). A possible explanation is that air temperature variations at seasonal time-scales have a more dominant role than seasonal emissivity changes.

TABLE I
CORRELATION COEFFICIENTS (R) BETWEEN THE SATELLITE (ESCAT-A AND SSM/I T_b) AND NCEP/NCAR (T_s AND P) FOR EACH OF THE SIX REGIONS OF INTEREST

	A		T_b	
	T_s	P	T_s	P
Ronne Ice Shelf	-0.24	-0.52	0.58	0.12
Palmer Land	0.09	-0.66	0.57	0.46
Thwaites Region	0.25	0.48	0.64	0.54
Amery Ice Shelf	-0.43	0.54	0.50	0.36
Queen Maud Land	0.13	-0.10	0.61	0.19
East Antarctica	-0.11	0.60	0.75	0.36

The observed relationships between A and T_b with T_s and P have been further validated by performing a correlation analysis for each of the six test sites in Fig. 3. The results are shown in Table I. There is a significant correlation between A and P ($|r| = 0.48$–0.66) for all areas except Queen Maud Land. It is interesting to note that for some regions, the correlation is positive and for others it is negative, which possibly reflects the influence of snow accumulation on firn with different physical properties, as shall be seen later in this paper. For all six test sites, we note a high and positive ($r = 0.5$–0.75) correlation between T_b and T_s. Over Palmer Land and Thwaites Region, we also note a significant correlation between T_b and P, which likely reflects a

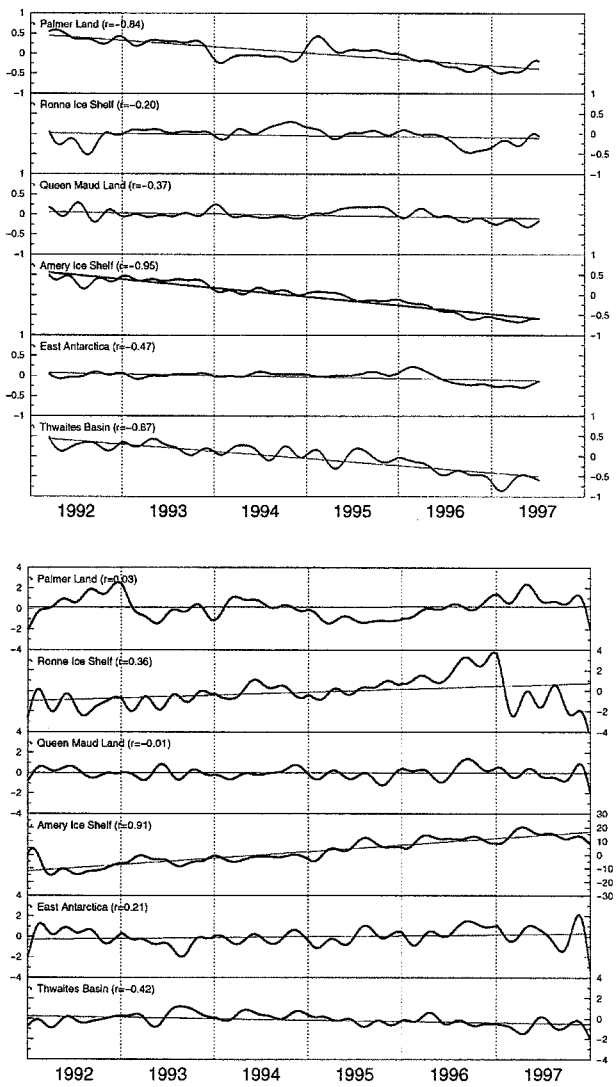

Fig. 8. Time-series anomalies of EScat A (in dB) (top) and SSM/I 19V T_b (in K) (bottom) for the six regions of interest shown in Fig. 3. A linear trend has been fitted to each profile and the corresponding correlation coefficient (r) computed.

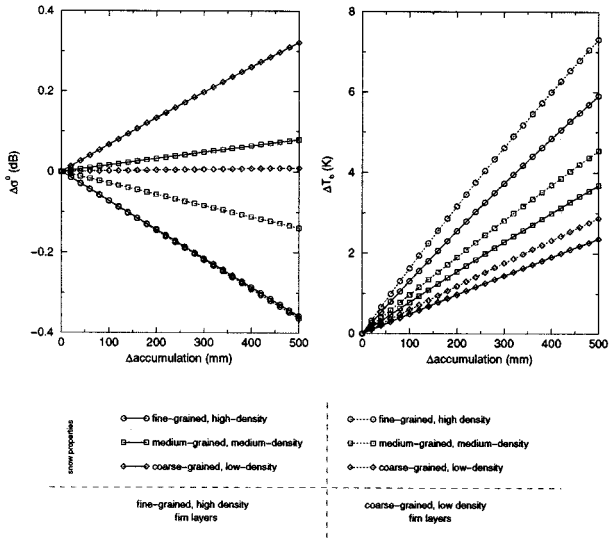

Fig. 9. Change in backscatter $(\Delta\sigma^0)$ and brightness temperature (ΔT_b) due to an increase in accumulation of snow consisting of different grain size and density. The solid lines indicate changes that occur due to snow accumulating on a firn pack consiting of fine-grained, high density firn layers. Dotted lines indicate changes that occur when the firn pack consists of coarse-grain, low density firn layers.

significant change in the emissivity due to changes in accumulation.

IV. Interannual Changes

Interannual changes in the microwave time-series data are best studied from the corresponding smoothed anomaly data. Fig. 8 shows the time-series anomalies of EScat-A and SSM/I 19V T_b for the six regions of interest (Fig. 3). In general, A anomalies have a negative trend. This is particularly significant for Palmer Land, Amery Ice Shelf, and Thwaites Region, which show an interannual trend of the order -0.2 dB yr^{-1} between 1992–97. T_b anomalies show a mostly positive interannual trend, although this is significant only over the Amery Ice Shelf, which experienced an increase in T_b of 4.8 K yr^{-1}.

We have already speculated that such interannual trends are likely caused by an increase in accumulation. The backscatter and brightness temperature models (2) and (3) can therefore be used to quantify the increase in accumulation required to explain these changes. Fig. 9 illustrates the modeled effect on A and T_b of adding a new snow layer (representing accumulation) with variable thickness on top of a multilayered firn pack. The model was computed for two different firn stratigraphies and for three different sets of new snow properties. One firn pack stratigraphy consisted of high density (5) fine-grain firn sizes ($r_0 = 0.4$ mm) and the other of low density (6) coarse-grain firn sizes ($r_0 = 0.7$ mm). We assume the firn stratigraphy remains constant during the period of snow accumulation. Three sets of new snow properties were used in order to characterize the condition in which the snow is precipitated. For example, snow deposited in windless conditions tends to consist of large, low density crystals, while in windy conditions, the accumulated snow is densely packed and small grained. In addition, we have assumed a crystal growth rate $K = 0.0001$ mm^2 yr^{-1} and layer thickness $D = 20$ mm.

The results indicate that enhanced deposition of high density, fine-grained snow, relative to the underlying firn, results in a reduction in A and large increases in T_b. On the other hand, enhanced deposition of low density, coarse-grained snow relative to the firn, results in an increase in A and a reduced increase in T_b. In the first scenario, A decreases because new high density, fine-grained snow attenuates radar energy both incident on and scattered from the underlying firn. While in the second scenario, A increases because the upper layer is a more efficient scatterer than the smaller-grained underlying firn. T_b increases in both scenarios because emissivity is sensitive to layer thickness [14].

The structure of the underlying firn also has a considerable effect on the change in A and T_b, due to accumulation. If the firn stratigraphy consists of low density, coarse-grained firn layers, then accumulation of any type of new snow will result in more negative changes in A and more positive changes in T_b than

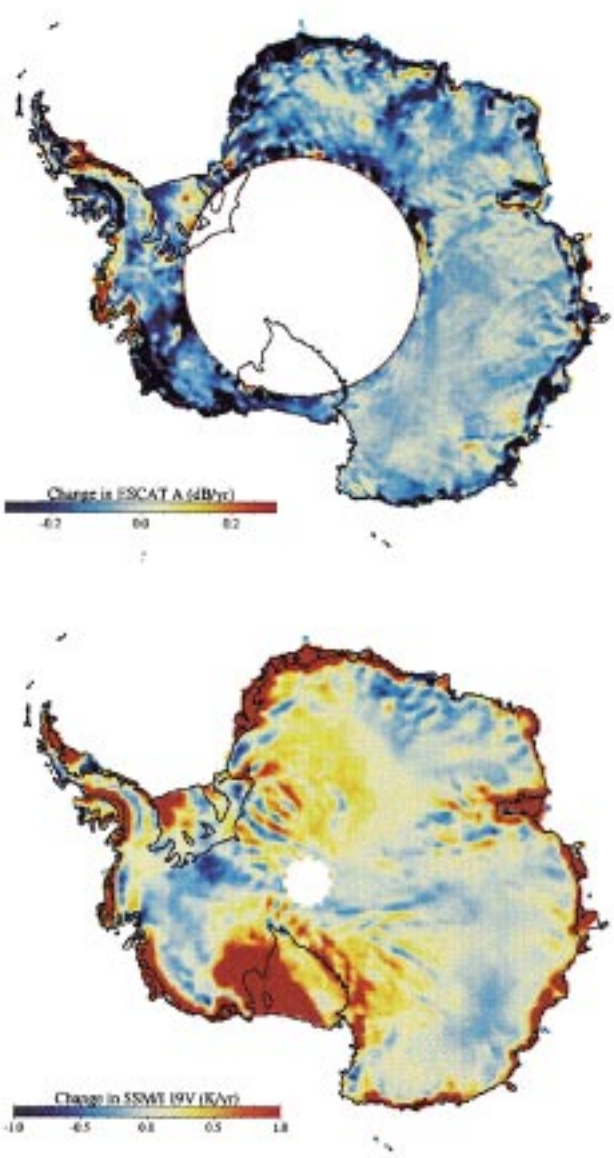

Fig. 10. Mean rate of change of EScat A (top) and SSM/I 19V T_b (bottom) signatures during the period 1992–1997.

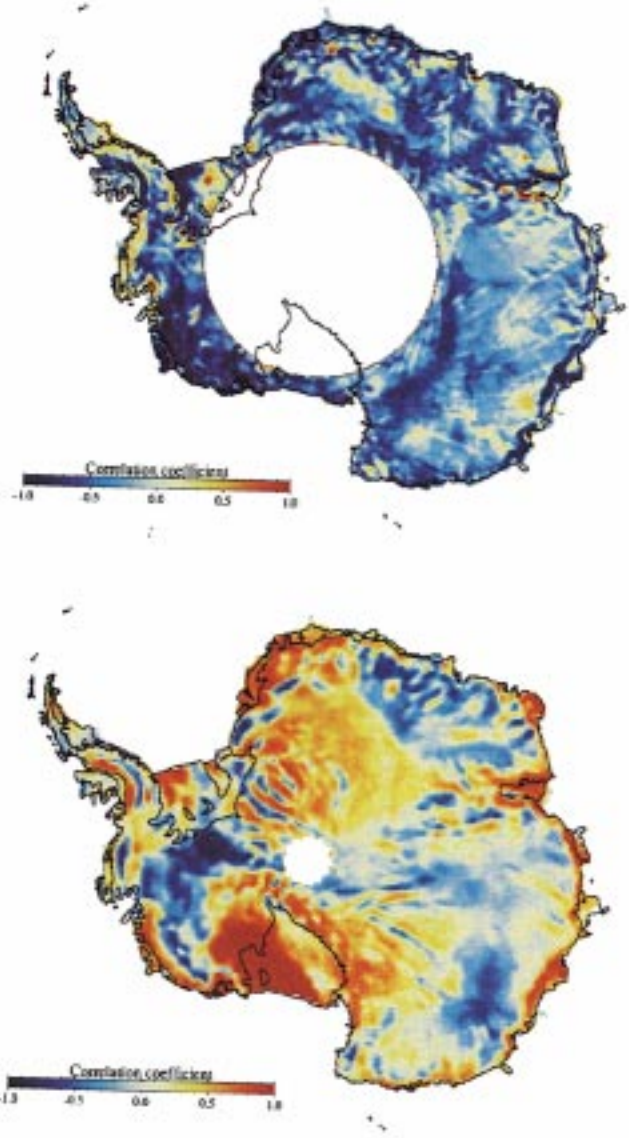

Fig. 11. Goodness of linear fit, expressed as a correlation coefficient of EScat A (top) and SSM/I 19V T_b (bottom) anomaly data for the period 1992–1997.

otherwise would be observed with high density, fine-grained firn layers. That is to say, accumulation will have a larger impact on A and T_b over regions with a well-developed scattering layer (for example, regions where melt and refreezing have occurred or where depth hoar exists).

The spatial variability in the mean rate of change in A and T_b over the entire Antarctic ice sheet and ice shelves during the period 1992–1997 are presented in Fig. 10. The images in this figure were produced by computing a trend in a linear fit to the time-series anomaly data on a pixel-by-pixel basis. The goodness of the linear fit to each set of pixel data are expressed as correlation coefficients (Fig. 11), and the variability of the anomaly data from the linear trend are expressed as root mean square (RMS) differences (Fig. 12).

The rate of change images (Fig. 10) indicate regions on the Antarctic ice sheet that experienced change in the surface properties and near surface scattering during 1992–1997. Regions of significant change are generally at the margins of the ice sheet and on ice shelves. This is particularly noticeable on the western edge of the Antarctic Peninsula and at the margins of the West Antarctic ice sheet (110° W to 160° W), Wilkes Land (100° E to 145° E) and Queen Maud Land (20° W to 30° E) (Fig. 3), where A indicates large negative trends ($< \ -0.25$ dB yr^{-1}) and T_b large positive trends (> 1 K yr^{-1}). Over these regions, the magnitude of the correlation coefficients (Fig. 11) are high, which implies the trends are significant. The RMS difference images (Fig. 12) show that for these regions, the RMS difference in A is comparable to other areas on the ice sheet, but for T_b, the magnitudes are generally larger. This implies that T_b anomalies

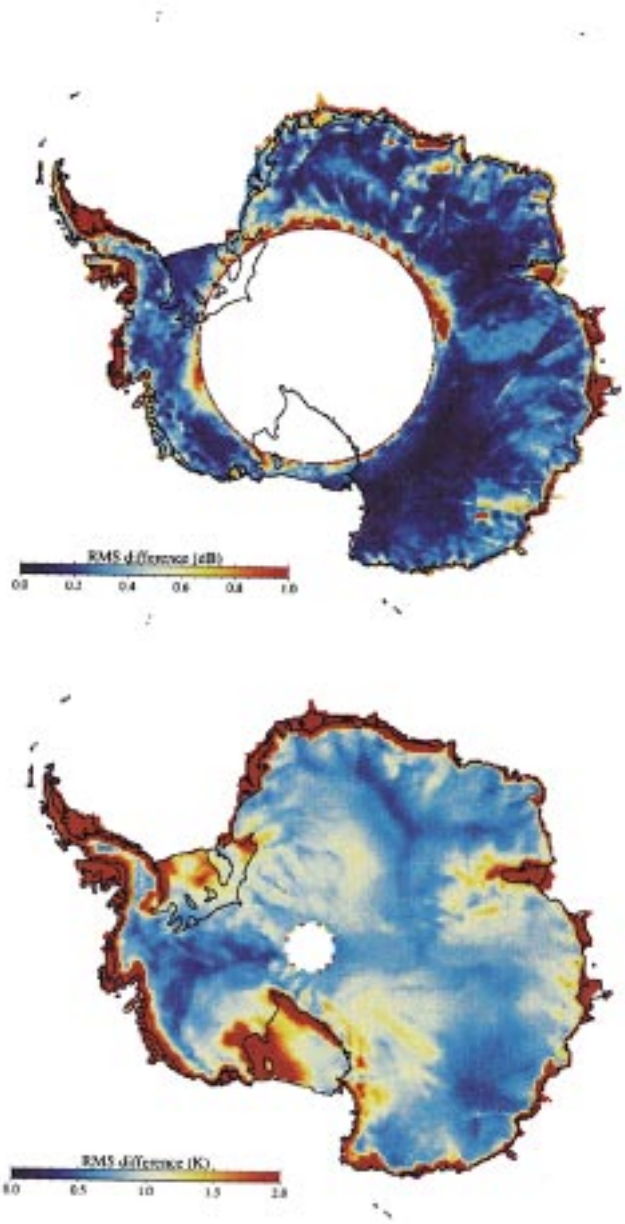

Fig. 12. RMS difference between EScat A anomaly data and linear fit (top) and RMS difference between SSM/I 19V T_b anomaly data and linear fit (bottom) for the period 1992–1997.

contain a high degree of seasonal variability superimposed upon the interannual trend, possibly as a result of seasonal temperature cycles.

It is also of interest to note that regions where significant trends are observed also have high accumulation rates (> 300 mm yr^{-1} [40]) and correspond with regions known to have experienced past melt events (see [26]). It is likely therefore, that the magnitude of the trends are enhanced in these regions because of the combination of two factors. First, relatively thick annual layers contribute to the change in A and T_b through enhanced absorption. Second, when a scattering layer is present in the underlying firn, which is typically the case after a melt event, the magnitude of the changes in A and T_b after snow accumulation is greater than if there was no

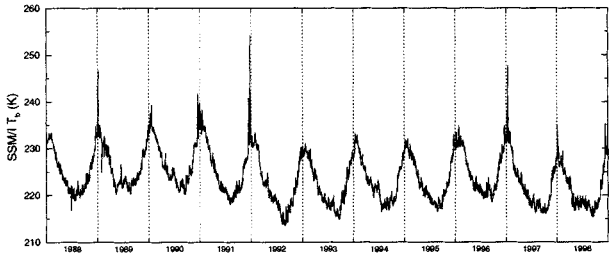

Fig. 13. SSM/I T_b of the Ronne Ice Shelf showing melt events in 1991–1992 and 1996–1997. Between these two dates, T_b increases interannually due to an increase in emissivity as the scattering layer, formed during refreezing after the 1991–1992 melt event, is buried by annual snow layers.

scattering layer present (as illustrated in Fig. 9). The results for T_b are also consistent with results for the Greenland ice sheet, which also shows the strongest trends over regions with accumulation typically about 300 mm yr^{-1} [20].

Other regions with significant trends are also observed in the rate of change images. For example, at elevations greater than 1500 m within the West Antarctic ice sheet, where no melting has occurred, there are local regions where A has a strong trend (< -0.2 dB yr^{-1}), but T_b shows no significant trend. A possible interpretation of this is that a depth hoar layer, consisting of coarse-grained crystals, exists at a depth penetrated at C-band frequencies (5.3 GHz) but not at K-band (19 GHz). To illustrate this point, imagine, for simplicity, an homogeneous firn layer with grain radii of 1 mm. According to Fig. 1, the penetration depth at C and K-band in dry firn is approximately 100 m and 10 m, respectively. If a hoar layer existed between these two depths, only EScat would be sensitive to the burial of this hoar layer.

If we were to extend the microwave record over a period of a few decades, it is likely a sawtooth pattern in the A and T_b time-series data would be observed. In this case, a step-response would occur in the data when a dominant scattering layer and significant stratigraphic marker is formed (during refreezing, after a melt-event, or during formation of depth-hoar) followed by linear change as the scattering layer is buried by successive annual snow layers. Part of this sequence is captured in Fig. 13, which shows that a melt event occurred on the Ronne Ice Shelf in 1991–92, immediately followed by a dramatic decrease in T_b. During the subsequent period leading up to 1996–97, when another melt event occurred, T_b increases interannually. A similar pattern is also observed in the other regions of interest. Melt events and hoar formation, therefore, introduce the analogy of a stratigraphic marker in the microwave record, which may be used to quantify accumulation if these layers are preserved.

V. Conclusions

In this paper, we have studied seasonal and interannual variability in EScat and SSM/I image data of the Antarctic ice sheet. Clear seasonal cycles are observed in both EScat A and SSM/I T_b time-series for all regions of study on the ice sheet. A data have seasonal amplitudes, typically, $\sim$0.5 dB and T_b data have seasonal amplitudes $\sim$10 K. We have demonstrated that these cycles are likely to be attributed to seasonal surface air temperature forcing, which has an impact on the dielectric properties

and physical temperature of the firn. In this study, analyses were confined to regions known to have negligible azimuthal modulation. Over regions where this is not the case, seasonal shifts in the wind direction may alter interface roughness orientation and/or ice crystal shapes, and contribute either constructively or destructively to the observed seasonal cycle. Further work is therefore required to establish to what extent azimuthal modulation can influence the seasonal cycle and what spatial patterns in firn characteristics lead to anisotropic scattering signatures.

Trends in A and T_b time-series data between 1992–1997 have been computed for the entire Antarctic ice sheet. Areas of greatest change (where $A < -0.25$ dB yr^{-1} and $T_b > 1$ K yr^{-1}) occur mainly at the margins of the ice sheet and on ice shelves where previous melt events have occurred and where accumulation is relatively high (> 300 mm yr^{-1}). Through our modeling efforts, we have demonstrated that the microwave signatures change because of the successive burial of a scattering layer formed after a melt event prior to 1992. This in turn leads to a net reduction in volume scattering and net increase in microwave emission from within the firn pack. These results suggest that the formation of a scattering layer (either by refreezing of liquid water or by development of hoar) can introduce the analogy of a stratigraphic marker in the microwave record which, in turn, may be used to quantify accumulation.

The results of this study indicate that to monitor long-term change in the properties of the Antarctic ice sheet, it is necessary to remove the seasonal cycle from time-series microwave data and thereby use anomaly data to understand the link between A and T_b with snow accumulation and wind shifts. The recent launch of the SeaWinds scatterometer on the QuikSCAT satellite in May 1999 now offers the potential of obtaining a long, uninterrupted time-series of daily, overlapping Antarctic Ku-band data at relatively higher resolution than C-band EScat. Since SeaWinds is a conically scanning instrument, the azimuthal diversity of the measurement data will allow azimuthal modulation effects to be removed from the climate-change data record. Moreover, QuikSCAT records both VV- and HH-polarized measurements and thus, together with EScat, the combination of frequencies and polarizations will enable electromagnetic scattering and emission properties of the surface to be studied more rigorously than is presently possible.

ACKNOWLEDGMENT

The authors would like to thank D. Long, Brigham Young University, Provo, UT, for the supply of SIRF-processed EScat data. They are also grateful to R. Bindschadler, W. Abdalati, and C. Shuman, whose insightful comments and suggestions significantly improved the content of this paper.

REFERENCES

[1] D. Vaughan and C. Doake, "Recent atmospheric warming and retreat of ice shelves on the Antarctic Peninsula," *Nature*, vol. 379, pp. 328–331, 1996.

[2] H. Rott, P. Skvarca, and T. Nagler, "Rapid collapse of northern Larsen ice shelf," *Science*, vol. 271, pp. 788–792, 1996.

[3] J. Ridley, "Surface melting on Antarctic peninsula ice shelves detected by passive microwave sensors," *Geophys. Res. Lett.*, vol. 20, no. 23, pp. 2639–2642, 1993.

[4] R. Bindschadler and P. Vornberger, "Changes in the west Antarctic ice sheet since 1963 from declassified satellite photography," *Science*, vol. 279, no. 5351, pp. 689–692, 1998.

[5] E. Rignot, "Fast recession of a west Antarcic glacier," *Science*, vol. 281, no. 5376, pp. 549–551, 1998.

[6] M. Drinkwater and D. Long, Seasat, EERS-1/2 and NSCAT scatterometer observed-changes in the large ice sheets, in Joint ESA—Eumetsat Workshop on Emerging Scatterometer Applications—From Research to Operations, Eur. Space Agency, ESTEC, Noordwijk, The Netherlands, no. SP-424, pp. 91–95, Oct. 5–7, 1998.

[7] J. Mercer, "West Antarctic ice sheet and CO_2 greenhouse: A threat of disaster," *Nature*, vol. 271, pp. 321–325, 1989.

[8] W. White and R. Peterson, "An Antarctic circumpolar wave in surface pressure, wind, temperature and sea-ice extent," *Nature*, vol. 380, 1996.

[9] H. Rott, Snow and ice monitoring by microwave techniques, in Alpbach Summer School, Eur. Space Agency, ESTEC, no. SP-205, pp. 75–86, 1983.

[10] K. Jezek, M. Drinkwater, J. Crawford, R. Bindschadler, and R. Kwok, "Analysis of synthetic aperture radar data collected over the southwestern Greenland ice sheet," *J. Glaciol.*, vol. 39, no. 131, pp. 119–132, 1993.

[11] D. Long, P. Hardin, and P. Whiting, "Resolution enhancement of spaceborne scatterometer data," *IEEE Trans. Geosci. Remote Sensing*, vol. 31, pp. 700–715, May 1993.

[12] D. Long and M. Drinkwater, "Greenland observed at high resolution by the Seasat-A scatterometer," *J. Glaciol.*, vol. 32, no. 2, pp. 213–230, 1994.

[13] C. Mätzler and R. Hüppi, "Review of signature studies for microwave remote sensing of snowpacks," *Adv. Space Res.*, vol. 9, no. 1, pp. 253–265, 1989.

[14] H. Zwally, "Microwave emissivity and accumulation rate of polar firn," *J. Glaciol.*, vol. 18, no. 79, pp. 195–215, 1977.

[15] H. Rott and K. Sturm, "Microwave signature measurement of Antarctic and Alpine snow," in *11th EARSeL Symposium*, Graz, Austria, 1991, pp. 140–151.

[16] W. Paterson, *The Physics of Glaciers*. Oxford, U.K.: Pergamon, 1994.

[17] A. Gow, "Snow studies in Antarctica," Tech. Rep. Res. Rep. 177, Cold Regions Res. Eng. Lab., Hanover, NH, 1965.

[18] C. Benson, "Stratigraphic studies in the snow at Byrd Station, Antarctica, compared with similar studies in Greenland," in *Antarctic Snow and Ice Studies II*, A. Crary, Ed. Washington, DC: Amer. Geophys. Union, 1971, vol. 16, pp. 333–353.

[19] R. Alley, "Concerning the deposition and diagenesis of strata in polar firn," *J. Glaciol.*, vol. 34, no. 118, pp. 283–290, 1988.

[20] W. Abdalati and K. Steffan, "Accumulation and hoar effects on microwave emission in the Greenland ice-sheet dry-snow zones," *J. Glaciol.*, vol. 44, no. 148, pp. 523–531, 1998.

[21] A. Bingham and M. Drinkwater, Backscatter characteristics of layered Antarctic firn, , to be published.

[22] M. Drinkwater, "LIMEX '87 ice surface characteristics: Implications for C-band SAR backscatter signatures," *IEEE Trans. Geosci. Remote Sensing*, vol. 27, pp. 501–513, Sept. 1989.

[23] C. Shuman and R. Alley, "Spatial and temporal characterization of hoar formation in central Greenland using SSM/I brightness temperatures," *Geophys. Res. Lett.*, vol. 20, no. 23, pp. 2643–2646, 1993.

[24] T. Mote and M. Anderson, "Variations in snowpack melt on the Greenland ice sheet based on passive microwave-measurements," *J. Glaciol.*, vol. 41, pp. 51–60, 1995.

[25] W. Abdalati and K. Steffen, "Snowmelt on the Greenland ice sheet as derived from passive microwave satellite data," *J. Climate*, vol. 10, no. 2, pp. 165–175, 1997.

[26] H. Zwally and S. Fiegles, "Extent and duration of Antarctic surface melting," *J. Glaciol.*, vol. 40, no. 136, pp. 463–476, 1994.

[27] M. Fahnestock, R. Bindschadler, R. Kwok, and K. Jezek, "Greenland ice sheet surface properties and ice dynamics from ERS-1 SAR imagery," *Science*, vol. 262, no. 5139, pp. 1530–1534, 1993.

[28] W. Rees, J. Dowdeswell, and A. Diament, "Analysis of ERS-1 synthetic aperture radar data from Nordaustlandet, Svalbard," *Int. J. Remote Sens.*, vol. 16, no. 5, pp. 905–924, 1995.

[29] D. Long and M. Drinkwater, "Cryosphere applications of NSCAT data," *IEEE Trans. Geosci. Remote Sensing*, vol. 37, pp. 1671–1684, May 1999.

[30] ——, "Azimuth variation in microwave data over Antarctica," *IEEE Trans. Geosci. Remote Sensing*, to be published.

[31] J. King and S. Harangozo, "Climate change in the western Antarctic Peninsula since 1945: Observations and possible causes," *Ann. Glaciol.*, vol. 27, pp. 571–575, 1998.

[32] C. Shuman, R. Alley, M. Fahnstock, P. Fawcett, R. Bindschadler, J. White, P. Grootes, S. Anandakrishnan, and C. Stearns, "Detection and monitoring of annual indicators and temperature trends at GISP2 using passive microwave remote sensing datas," *J. Geophys. Phys.*, vol. 102, no. C12, pp. 26877–26 886, 1997.
[33] M. Hallikainen and D. Winebrenner, "The physical basis for sea ice remote sensing," in *Microwave Remote Sensing of Sea Ice*, F. Carsey, Ed. Washington, DC: Amer. Geophys. Union, 1992, pp. 29–46.
[34] C. Livingstone and M. Drinkwater, "Springtime C-band SAR backscatter signatures of Labrador Sea marginal ice: Measurements versus modeling predictions," *IEEE Trans. Geosci. Remote Sensing*, vol. 29, pp. 29–41, Jan. 1991.
[35] M. Tiuri, A. Sihvola, E. Nyfors, and M. Hallikainen, "The complex dielectric constant of snow at microwave frequencies," *IEEE J. Oceanic Eng.*, vol. OE-9, pp. 377–382, May 1984.
[36] W. Burke, T. Schmugge, and J. Paris, "Comparison of 2.8- and 21-cm microwave radiometer observations over soils with emission model calculations," *J. Geophys. Res.*, vol. 84, no. C1, pp. 287–294, 1979.
[37] R. Alley, J. Bolzan, and I. Whillans, "Polar firn densification and grain growth," *Ann. Glaciol.*, vol. 3, pp. 7–11, 1982.
[38] M. Sturm, J. Holmgren, M. Kömig, and K. Morris, "The thermal conductivity of seasonal snow," *J. Glaciol.*, vol. 43, no. 143, pp. 26–41, 1997.
[39] M. Higham and M. Craven, "Surface mass balance and snow surface properties from the Lambert Glacier Basin traverses 1990–94," Tech. Rep. Res. Rep. 9, Antarctic CRC, Hobart, Australia, 1997.
[40] R. Cullather, D. Bromwich, and M. Van Woert, "Spatial and temporal variability of Antarctic precipitation from atmospheric methods," *J. Climate*, vol. 11, no. 3, pp. 334–367, 1998.
[41] Eur. Space Agency, Noordwijk, The Netherlands, 1999.

Andrew Bingham received the B.Eng. degree in electrical and electronic engineering from the University of Plymouth, Plymouth, U.K., in 1989, the M.Sc. degree in remote sensing and image processing from the University of Edinburgh, Edinburgh, U.K., in 1990, and the Ph.D. degree in remote sensing and glaciology from the University of Cambridge, Cambridge, U.K., in 1997.

He was a Research Assistant with the University of Oxford, Oxford, U.K. from 1990 to 1993. Currently, he is an NRC Research Associate, NASA Jet Propulsion Laboratory (JPL), California Institue of Technology, Pasadena. His research interests include microwave remote sensing of ice sheets and glaciers for glaciological and climate related studies.

Mark R. Drinkwater (M'88) was born in Oldham, U.K., in 1963. He received the B.Sc. degree (with honors) from Durham University, Durham, U.K., in 1984, specializing in remote sensing in glaciology, and a Council of Europe Diploma in remote sensing in engineering from the University of Dundee, Dundee, U.K., in 1984. For his doctorate research, he studied at Emmanuel College, Cambridge, U.K., and the Scott Polar Research Institute, University of Cambridge, where he received the Ph.D. degree in geophysics in 1988.

From 1987 to 1988, he was a Consulting Research Scientist with Polar Oceans Associates, Cambridge, a Division of Science Applications International Corporation. In 1988, he was awarded a National Research Council Resident Research Associateship, and until 1990, he was with the Polar Oceanography Group, Jet Propulsion Laboratory (JPL), California Institute of Technology, Pasadena. From 1990 to 2000, he was a Research Scientist with the Ocean Sciences Research Element, JPL, working on several international projects with NASA, ESA, CSA, and NASDA. Since May 2000, he has been with the European Space Agency (ESA), where he is Head of the Oceans/Sea-Ice Unit of the Earth Sciences Division, European Space Research and Technology Centre (ESTEC), Noordwijk, The Netherlands. He has published over 40 refereed journal articles, several book chapters, and over 40 conference papers. His professional interests involve microwave remote sensing of the polar oceans and terrestrial ice sheets. Recent focuses include geophysical data extraction, inverse electromagnetic scattering, and coupling EM and thermodynamic models with massively parallel general circulation models for large-scale estimates of surface fluxes of heat and salt in the polar oceans.

Dr. Drinkwater is a member of the International Glaciological Society, the IEEE Geoscience and Remote Sensing Society, and was recently an Associate Editor of the American Geophysical Union's *Journal of Geophysical Research, Oceans*.